

Scaling theory of fading ergodicity

Rafał Świątek,^{1,2} Miroslav Hopjan,¹ Carlo Vanoni,^{3,4} Antonello Scardicchio,^{5,6} and Lev Vidmar^{1,2}

¹*Department of Theoretical Physics, J. Stefan Institute, SI-1000 Ljubljana, Slovenia*

²*Department of Physics, Faculty of Mathematics and Physics, University of Ljubljana, SI-1000 Ljubljana, Slovenia*

³*SISSA – International School for Advanced Studies, via Bonomea 265, 34136, Trieste, Italy*

⁴*Department of Physics, Princeton University, Princeton, New Jersey, 08544, USA*

⁵*INFN Sezione di Trieste, Via Valerio 2, 34127 Trieste, Italy*

⁶*ICTP, Strada Costiera 11, 34151, Trieste, Italy*

In most noninteracting quantum systems, the scaling theory of localization predicts one-parameter scaling flow in both ergodic and localized regimes. On the other hand, it is expected that the one-parameter scaling hypothesis breaks down for interacting systems that exhibit the many-body ergodicity breaking transition. Here we introduce a scaling theory of fading ergodicity, which is a precursor regime of many-body ergodicity breaking. We argue that the two-parameter scaling governs the entire ergodic regime; however, (i) it evolves into the one-parameter scaling at the ergodicity breaking critical point with the critical exponent $\nu = 1$, and (ii) it gives rise to the resilient one-parameter scaling close to the ETH point. Our theoretical framework may serve as a building block for two-parameter scaling theories of many-body systems.

Introduction.— The emergence of thermalization in isolated quantum many-body systems has attracted considerable attention since the beginning of quantum mechanics. While it is nowadays understood that in most isolated quantum many-body systems, local observables approach the thermal ensemble predictions after being taken out of equilibrium [1–11], much less is known about typical (as opposed to integrable) systems that avoid thermalization in the thermodynamic limit. If, upon tuning a parameter, the system can be made to switch from a thermal to a non-thermal phase, of particular importance becomes the understanding of the critical behavior at the boundary, and its relationship to other critical phenomena such as ground-state quantum phase transitions [12] or spin-glass transitions [13, 14].

Since most of the studies are carried out in finite systems, the central question concerns how the properties of those systems flow with increasing the system size either towards ergodicity, for which the eigenstate thermalization hypothesis (ETH) represents a fixed point [1–5], or towards localization, which is another fixed point. A paradigmatic example of the latter is Anderson localization [15], which became a hallmark of ergodicity breaking in noninteracting quantum systems. A milestone in the understanding of Anderson transition in finite-dimensional lattices has been the scaling theory by Abrahams, Anderson, Licciardello, and Ramakrishnan [16], which is based on the one-parameter scaling hypothesis, investigated numerically by later studies [17, 18]. Recent studies have further developed this theoretical framework using modern observables, e.g., the spectral statistics, the wavefunction fractal dimension and entanglement entropy [19–31], and they explored its validity and limitations in special geometries, such as random regular graphs [30, 32–36]. In such graphs, it was found [31] (see also [35, 36]) that the one-parameter scaling hypothesis is not sufficient, and one needs to resort to a two-parameter scaling theory, similar in many ways to what describes the Kosterlitz-Thouless transition [37].

A common perspective on many-body quantum systems, which are candidates for ergodicity breaking, is that they exhibit many analogies with the Anderson model on expander graphs [30, 36, 38–40]. Yet, they do not seem to be governed by the one-parameter scaling hypothesis. The evidence supporting this expectation is diverse [41–45], and in most cases, it is obtained by studying the random-field XXZ model [41, 42, 46–50], see [51] for a recent example. In the latter model, the many-body ergodicity-breaking transition is the many-body localization transition [11, 52–56].

Recent work has introduced a scenario of many-body ergodicity breaking dubbed fading ergodicity [57]. It represents a precursor regime of ergodicity breaking that is still ergodic, despite ETH ceasing to be valid in its conventional form [3, 4, 58]. The toy model of fading ergodicity is the quantum sun model [59, 60], which is closely connected to the avalanche theory in spin-1/2 chains [59–71]. The ergodicity breaking transition in the quantum sun model is better controlled at the theoretical level than that of the random-field XXZ model, and, at the same time, shows less puzzling finite-size effects. This makes one suspect that the scaling theory of fading ergodicity, and the corresponding renormalization group (RG) flow, are different from those of the random-field XXZ model.

Indeed, in this Letter we introduce a theoretical framework that allows us to describe the two-parameter flow of fading ergodicity, showing that it is a different scenario from that depicted by the random-field XXZ model, and presenting a new universality class of ergodicity-breaking transitions.

In particular, studying the entanglement properties of many-body quantum states, we inspect the flow towards the two special points, i.e., the ergodicity breaking critical point [59, 60, 70] and the ETH fixed point [57]. We argue that the two-parameter description contains a rather simple structure. It evolves into a one-parameter description at the critical point with the critical exponent $\nu = 1$, and it exhibits a resilient one-parameter descrip-

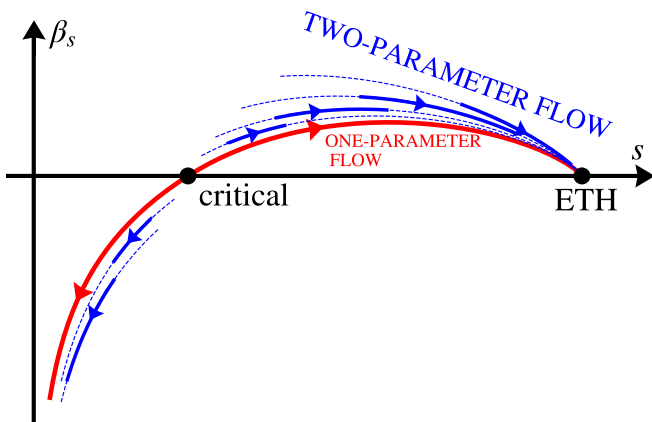


FIG. 1. Two-parameter scaling of fading ergodicity. Dashed blue lines are results for the beta function β_s from Eq. (8) at different interactions α , and the overlapping solid blue lines are results for the numerically available system sizes L . The solid red line is the critical one-parameter flow with the critical exponent $\nu = 1$, *i.e.*, Eq. (8) with $a = a_0$. The two-parameter flows in the ergodic phase terminate, with the same derivative, at the ETH fixed point $s = 1$.

tion when approaching the ETH fixed point, giving rise to the matching derivatives of different beta functions at the ETH fixed point, as sketched in Fig. 1.

Set-up.— In the quantum sun model [59, 65], a central “sun”, *i.e.*, a quantum dot of dimension 2^N (with fixed $N = 3$ in our case), is connected with L rays of increasing length u_ℓ to as many spin-1/2 qubits which are subject to random field of $O(1)$ strength. Two parameters are needed to describe this Hamiltonian: the interaction $\alpha \in [0, 1]$ that determines the decay factor for each spin coupling (which is proportional to α^{u_ℓ}), and the overall interaction strength g_0 , see Eq. (14) in End Matter for details. A critical α_c separates an ergodic phase at $\alpha > \alpha_c$ from a localized phase at $\alpha < \alpha_c$, with $\alpha_c \approx 1/\sqrt{2}$ (the numerical value of α_c , however, is slightly larger than $1/\sqrt{2}$ and it weakly depends on g_0). Fading ergodicity is observed at $\alpha_c < \alpha \lesssim 1$, while the observable fluctuations are close to those predicted by the conventional ETH at $\alpha \approx 1$ [57].

We identify the single-site entanglement entropy as an observable with well-defined properties in the ergodic and localized regimes. We consider the bipartite entanglement entropy in an eigenstate $|n\rangle$, partitioned into a subsystem A , being a single spin at $j = L$ distance from the “sun”, and its complement B . We define the reduced density matrix as $\hat{\rho}_A^n = \text{Tr}_B |n\rangle\langle n|$ and compute the von Neumann entanglement entropy $S_A^n = -\text{Tr}(\hat{\rho}_A^n \ln \hat{\rho}_A^n)$, which we average over eigenstates in a microcanonical energy window at the mean total energy, denoted as \bar{S}_A . We define the scaled average entanglement entropy as $s = \bar{S}_A/S_A^{\max}$, where $S_A^{\max} = \ln 2$ is the maximal entropy. This quantity interpolates between the localized phase, $s \rightarrow 0$, and the ergodic phase, $s \rightarrow 1$.

Beta function.— The goal of the Letter is to study the

scaling properties of s in terms of the beta function,

$$\beta_s = \frac{d \ln s}{d \ln L}. \quad (1)$$

While the beta function was originally introduced for the dimensionless conductance [16], we consider here the beta function of the wavefunction entanglement entropy. For the latter (and also for other indicators such as the wavefunction fractal dimension or spectral statistics [30, 31, 72]), the beta function β_s displays three fixed points: the ergodic (ETH) fixed point at $s = 1$, the localized fixed point at $s = 0$, and a third isolated zero at the critical point s_c (Wilson-Fisher fixed point), with $0 < s_c < 1$.

When a critical point $\alpha = \alpha_c$ is described by a one-parameter scaling, the beta function is expected to display power-law corrections $L^{-\gamma}$ to the critical entanglement entropy $s = s_c$. In the vicinity of the critical point, one can linearize the beta function,

$$\beta_s = b_0(s - s_c) + O((s - s_c)^2), \quad (2)$$

such that $b_0 = \beta'_s$ at $s = s_c$. Solving Eq. (2) for s produces the scaling relation

$$s(L) = s_c + f((L/\xi)^{1/\nu}), \quad (3)$$

where ν is the critical exponent, $\nu = 1/(s_c b_0)$, and $f(z)$ is a scaling function that is linear for small z [51]. The correlation/localization length ξ diverges at the critical point. Previous work studied numerical scaling collapses in the spirit of Eq. (3) for the level spacing ratio [59, 70], and in End Matter we show similar scaling collapses for s .

Scaling arguments.— Let us first focus on the behavior of the beta function Eq. (1) in the fading ergodicity regime. To do so, we need to describe the dependence of s on the linear size L in the region of interest. We start by observing that the approach to the ETH fixed point $s = 1$ is governed by random-matrix theory corrections of the form $s \simeq 1 - c/D + O(D^{-2})$, where $D \propto 2^L$ is the Hilbert-space dimension. Such corrections are typical for Haar-random pure states [73], see [74] for a detailed calculation. However, in the fading ergodicity regime [57], one expects the corrections to the maximal value of the entanglement entropy s to scale as

$$s \simeq 1 - \frac{c}{D_{\text{eff}}} + O(D_{\text{eff}}^{-2}) = 1 - ce^{-L/\eta} + O(e^{-2L/\eta}), \quad (4)$$

with the fluctuation exponent η depending on α , and approaching $\eta = 1/\ln 2$ at the ETH point ($\alpha \rightarrow 1$) and $\eta \rightarrow \infty$ at the ergodicity breaking critical point ($\alpha \rightarrow \alpha_c$). The ansatz in Eq. (4) is motivated by the similarity of the scaling properties of the single-site entanglement entropies and the variances of the matrix elements of observables from Ref. [57], see [74] for details. Indeed, it was argued [57] that the fluctuation exponent η scales as $\eta = 1/\ln 2(1 - \ln \alpha/\ln \alpha_c)^{-1}$, up to constant prefactor.

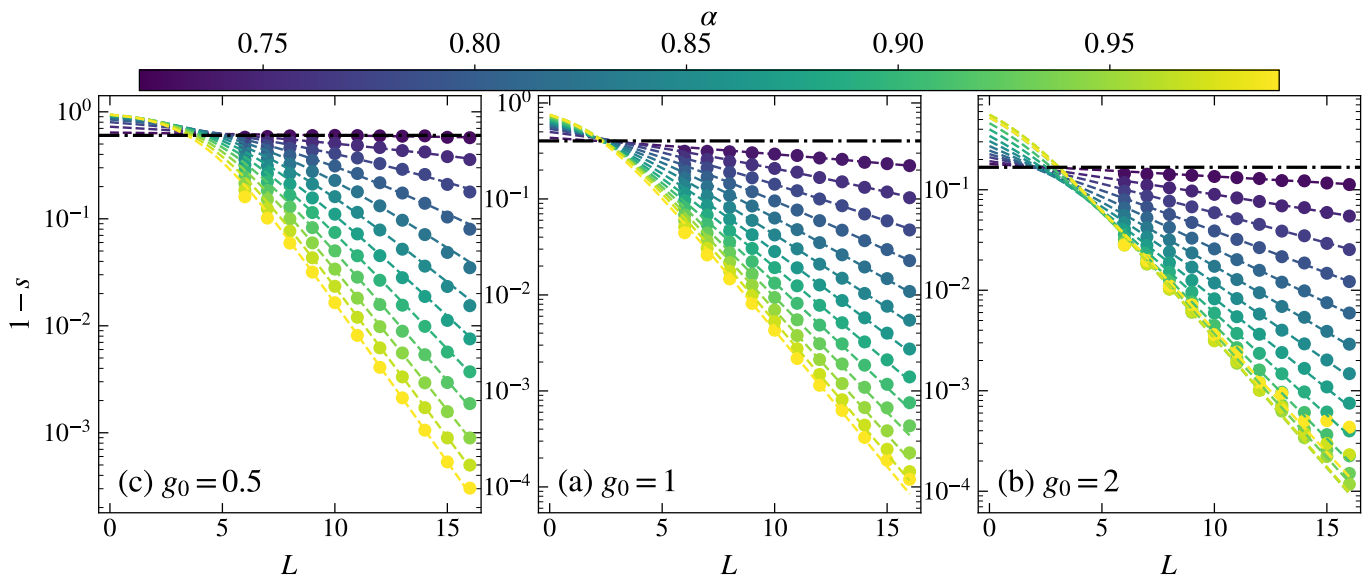


FIG. 2. Symbols: Numerical results for $1-s$ in the ergodic phase at (a) $g_0 = 0.5$, (b) $g_0 = 1$, and (c) $g_0 = 2$. Dashed lines are fits using Eq. (7), for system sizes $L > 9$, with free parameters a and η . The horizontal dash-dotted lines are the values $1-s_c$ at the critical point.

Hence, it diverges at the critical point and it assumes the role of ξ from Eq. (3).

The scaling ansatz from Eq. (4) corresponds to the following beta function, keeping only the first two terms in the expansion in powers of $1-s$:

$$\begin{aligned} \beta_{\text{fading}}(s, c) &= -\frac{1-s}{s} \ln(1-s) + \frac{1-s}{s} \ln(c) \\ &= -(1-s) \ln(1-s) + (1-s) \ln(c) + \\ &\quad + O((1-s)^2 \ln(1-s)). \end{aligned} \quad (5)$$

Notice that the above expression does not contain an explicit dependence on η , which enters as the initial condition, while c can attain dependence on model parameters, $c = c(\alpha) = c(s, L)$.

However, for a complete description of the RG flow of the quantum sun model, we need to incorporate also the behavior in the localized phase. Similarly to the fractal dimension in the Anderson model and to other spectral observables [30], the entanglement entropy decreases exponentially as $s \sim B e^{-L/\eta_{\text{loc}}}$ in the localized phase. This behavior corresponds to a beta function

$$\beta_{\text{loc}} \approx \ln s - \ln B + O(s \ln s), \quad (6)$$

which is consistent with the localized fixed point being $\beta(s \rightarrow 0) \rightarrow -\infty$. Again, the constant B can be dependent on the interaction α , leading to a two-parameter flow.

Following similar arguments as presented in [16], we argue that the beta function in Eqs. (5) and (6) indeed ensures the ergodicity breaking transition at finite s_c . On the ergodic side, the beta function approaches the ETH fixed point with a negative derivative (*i.e.*, from above),

while close to the localized fixed point it is negative. Consequently, there has to occur a sign change in the beta function at $s_c = s(\alpha_c)$, where $0 < \alpha_c < 1$, determining the transition from ergodicity to localization, see Fig. 1.

The specific scaling behaviors on the ergodic and localized sides discussed so far can be modeled as limiting cases to a general function. Here, we propose that the entanglement entropy can be modeled for any value of interaction as

$$s(L) = \frac{1}{1 + a e^{-L/\eta}}, \quad (7)$$

which incorporates both the ergodic, $\eta > 0$, and localized, $\eta = -\eta_{\text{loc}} < 0$, limiting cases. We demonstrate this ansatz in Fig. 2 for various values of $\alpha > \alpha_c$ (at $g_0 = 0.5, 1, 2$), and in Fig. 5 of End Matter for various values of $\alpha < \alpha_c$ (at $g_0 = 1$). Remarkably, the scaling function in Eq. (7) serves as a very robust fit up to small system sizes. Following Eq. (7) one is able to find the beta function, which takes the form

$$\beta_s(s, a) = -(1-s) \ln \frac{1-s}{s} + (1-s) \ln a. \quad (8)$$

Remarkably, β_s in Eq. (8) corresponds in the limits $s \rightarrow 1$ and $s \rightarrow 0$ to the beta functions in Eqs. (5) and (6), respectively. The critical point is $s_c = 1/(1+a)$ as it is easily seen either by solving $\beta_s(s, a) = 0$ or by letting $\eta \rightarrow \infty$ in Eq. (7). Then, one can calculate the slope of the beta function at $s = s_c$, which equals $\beta'_s(s = s_c, a) = 1/s_c$. As a consequence, the critical exponent in Eq. (3) equals

$$\nu = (\beta'_s(s_c))^{-1} = 1. \quad (9)$$

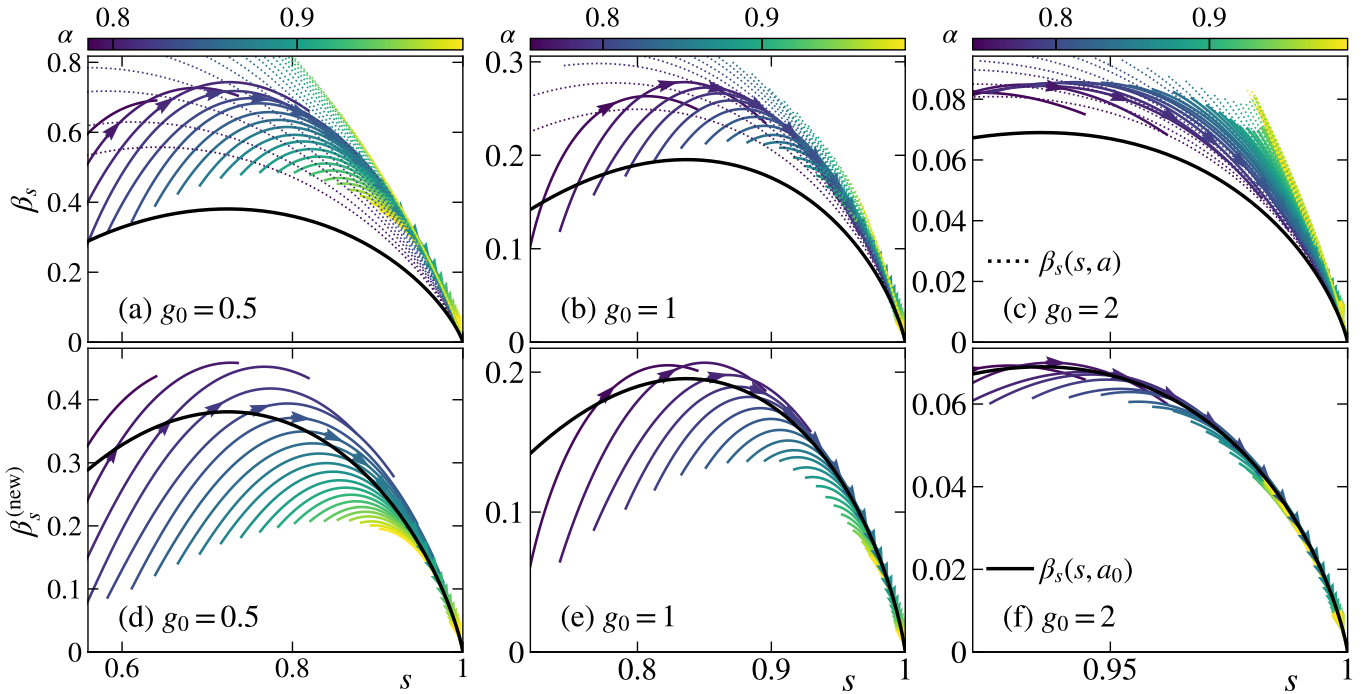


FIG. 3. (a-c) Numerical results for β_s in the ergodic phase at (a) $g_0 = 0.5$, (b) $g_0 = 1$, and (c) $g_0 = 2.0$, see [74] for details of numerical calculations. The arrows indicate the increase in system size $L = 7, \dots, 16$, and the colors denote the value of interaction α . Dotted lines show the two-parameter functions $\beta_s(s, a)$ from Eq. (8), with values of a extracted from Fig. 2, while the solid black line shows the one-parameter function $\beta_s(s, a = a_0)$. (d-f) Numerical results for $\beta_s^{(\text{new})}$ in Eq. (10), where the value of L_0 is estimated from the fits in Fig. 2, and the solid black line is again $\beta_s(s, a = a_0)$.

This family of $\beta_s(s, a)$ all have $\nu = 1$, irrespective of g_0 , *i.e.*, of the value of s_c . This result is consistent with previous studies [59, 61, 66], *e.g.*, with the divergence of Thouless conductance (the ratio of the Heisenberg and Thouless times) close to the critical point [59]. In fact, the Thouless conductance was shown to diverge as $\propto e^{L/\eta}$, with η introduced above.

Corrections to one-parameter scaling in the ergodic phase.— Despite the simple prediction for the critical exponent ν in Eq. (9), the beta function $\beta_s(s, a)$ in Eq. (8) still describes a two-parameter scaling since $a = a(\alpha) = a(s, L)$. We estimate its proximity to one-parameter scaling from the numerical results in Fig. 2. In the latter, the fitting functions to $1 - s$ vs L cross the horizontal dashed-dotted line at $L = L_0 = O(1)$, which is, to a reasonable approximation, independent of α . This suggests a possible parametrization of a from Eq. (7) as $a = a_0 \exp\{L_0/\eta\}$, where $a_0 = 1/s_c - 1$ is a constant at $\alpha = \alpha_c$. Then, by introducing a new variable $L' = L - L_0$, one defines the new beta function $\beta_s^{(\text{new})}$,

$$\beta_s^{(\text{new})} = \frac{d \ln s}{d \ln L'} = \left(1 - \frac{L_0}{L}\right) \beta_s(s, a), \quad (10)$$

which is the one-parameter beta function $\beta_s^{(\text{new})} = \beta_s(s, a_0)$, *i.e.*, the function in Eq. (8) at $a = a_0$. Hence, one can express $\beta_s(s, a) = \beta_s(s, L)$, our quantity of inter-

est, as

$$\beta_s(s, L) = \beta_s(s; a_0) \left(1 - \frac{L_0}{L}\right)^{-1}, \quad (11)$$

which at $L \gg L_0$ becomes

$$\beta_s(s, L) = \beta_s(s; a_0) + \frac{\beta_s(s; a_0) L_0}{L}, \quad (12)$$

i.e., a sum of the one-parameter scaling part and the two-parameter scaling part. This result suggests interesting consequences. For example, the beta functions β_s at different α exhibit the same slope, $\beta'_s = -\infty$, for all α at the ETH fixed point $s = 1$ (when $L_0/L \rightarrow 0$), but different slopes at $s < 1$. We interpret the behavior close to the ETH fixed point as a resilient one-parameter scaling. Moreover, the expression in Eq. (11) allows us to estimate the corrections to the critical exponent as

$$\nu = (\beta'_s(s_c) s_c)^{-1} = 1 - \frac{L_0}{L}, \quad (13)$$

which is further explored numerically in Fig. 4 of End Matter.

Numerical tests.— Our theoretical framework predicts that β_s is a two-parameter function and $\beta_s^{(\text{new})}$ is a one-parameter function. Figure 3 clearly confirms this prediction at $g_0 = 2$, see Figs. 3(c) and 3(f). We expect this behavior to be an asymptotic feature of the model. This observation is consistent with previous work that reported

the numerical value of the critical point at $g_0 > 1$ to be close to the analytically predicted value, $\alpha_c = 1/\sqrt{2}$ [60].

Decreasing g_0 , however, the numerical distinction between the one- and two-parameter scalings becomes less clear, see, e.g., the results at $g_0 = 0.5$ in Figs. 3(a) and 3(d). They appear to be consistent with one-parameter scaling of both β_s and $\beta_s^{(\text{new})}$, which is inconsistent due to their mutual relation in Eq. (10). At small $g_0 < 1$, the numerically extracted critical point is considerably larger than $\alpha_c = 1/\sqrt{2}$, see [60] and Fig. 4(a). We interpret this property, together with the observations in Fig. 3, as evidence of significant finite-size effects in the $g_0 < 1$ regime.

Conclusions.— In this Letter, we studied a new universality class of ergodicity-breaking transitions. It is described by the framework of fading ergodicity [57], i.e., a precursor regime of ergodicity breaking in which volumic fluctuations of observables are gradually transformed to linear fluctuations at the critical point.

The phenomenology of fading ergodicity differs from the one in noninteracting systems that exhibit single-parameter scaling, and possibly also from the well-studied interacting models such as the random-field XXZ model. We showed that the beta function in the ergodic regime obeys, at large system sizes, the two-parameter scaling. However, the one-parameter scaling description is relevant in two opposite limits: it emerges in the vicinity of the critical point, and it gives rise to a simple structure near the ETH fixed point at $L \gg L_0$, where L_0 is a characteristic length associated to ergodization. We conjecture that the two-parameter flow of the random-field

XXZ model is connected to the latter by taking $L_0 \rightarrow \infty$. Our theoretical framework allows for identifying the critical exponent of fading ergodicity $\nu = 1$, and it offers a reference point for future explorations of alternative scenarios of ergodicity breaking.

ACKNOWLEDGMENTS

We acknowledge discussions with B. Altshuler, A. Chandran, V. Kravtsov and P. Sierant. R.S., M.H., and L.V. acknowledge support from the Slovenian Research and Innovation Agency (ARIS), Research core funding Grants No. P1-0044, No. N1-0273, No. J1-50005, and No. N1-0369, as well as the Consolidator Grant Boundary-101126364 of the European Research Council (ERC). C.V. and L.V. acknowledge the Simons Center for Geometry and Physics at Stony Brook for hospitality during part of the work on this project. The work of A.S. was funded by the European Union - NextGenerationEU under the project NRRP “National Centre for HPC, Big Data and Quantum Computing (HPC)”CN00000013 (CUP D43C22001240001) [MUR Decree n. 341- 15/03/2022] - Cascade Call launched by SPOKE 10 POLIMI: “CQEB” project, and by the PNR MUR project PE0000023-NQSTI.. We gratefully acknowledge the High Performance Computing Research Infrastructure Eastern Region (HCP RIVR) consortium [75] and European High Performance Computing Joint Undertaking (EuroHPC JU) [76] for funding this research by providing computing resources of the HPC system Vega at the Institute of Information sciences [77].

-
- [1] J. M. Deutsch, Quantum statistical mechanics in a closed system, *Phys. Rev. A* **43**, 2046 (1991).
 - [2] M. Srednicki, Chaos and quantum thermalization, *Phys. Rev. E* **50**, 888 (1994).
 - [3] M. Srednicki, The approach to thermal equilibrium in quantized chaotic systems, *J. Phys. A* **32**, 1163 (1999).
 - [4] M. Rigol, V. Dunjko, and M. Olshanii, Thermalization and its mechanism for generic isolated quantum systems, *Nature (London)* **452**, 854 (2008).
 - [5] L. D’Alessio, Y. Kafri, A. Polkovnikov, and M. Rigol, From quantum chaos and eigenstate thermalization to statistical mechanics and thermodynamics, *Adv. Phys.* **65**, 239 (2016).
 - [6] T. Mori, T. N. Ikeda, E. Kaminishi, and M. Ueda, Thermalization and prethermalization in isolated quantum systems: a theoretical overview, *J. Phys. B* **51**, 112001 (2018).
 - [7] J. M. Deutsch, Eigenstate thermalization hypothesis, *Rep. Prog. Phys.* **81**, 082001 (2018).
 - [8] S. Trotzky, Y.-A. Chen, A. Flesch, I. P. McCulloch, U. Schollwöck, J. Eisert, and I. Bloch, Probing the relaxation towards equilibrium in an isolated strongly correlated 1D Bose gas, *Nat. Phys.* **8**, 325 (2012).
 - [9] T. Langen, R. Geiger, M. Kuhnert, B. Rauer, and J. Schmiedmayer, Local emergence of thermal correlations in an isolated quantum many-body system, *Nature Physics* **9**, 640 (2013).
 - [10] J. Eisert, M. Friesdorf, and C. Gogolin, Quantum many-body systems out of equilibrium, *Nat. Phys.* **11**, 124 (2015).
 - [11] P. Sierant, M. Lewenstein, A. Scardicchio, L. Vidmar, and J. Zakrzewski, Many-body localization in the age of classical computing, [arXiv:2403.07111](https://arxiv.org/abs/2403.07111) (2024). 2403.07111.
 - [12] S. Sachdev, *Quantum Phase Transitions* (Cambridge University Press, New York, 2011).
 - [13] K. Binder and A. P. Young, Spin glasses: Experimental facts, theoretical concepts, and open questions, *Reviews of Modern physics* **58**, 801 (1986).
 - [14] M. Mézard, G. Parisi, and M. A. Virasoro, *Spin glass theory and beyond: An Introduction to the Replica Method and Its Applications*, volume 9 (World Scientific Publishing Company, 1987).
 - [15] P. W. Anderson, Absence of Diffusion in Certain Random Lattices, *Phys. Rev.* **109**, 1492 (1958).
 - [16] E. Abrahams, P. W. Anderson, D. C. Licciardello, and T. V. Ramakrishnan, Scaling theory of localization: Ab-

- sence of quantum diffusion in two dimensions, *Phys. Rev. Lett.* **42**, 673 (1979).
- [17] A. MacKinnon and B. Kramer, One-parameter scaling of localization length and conductance in disordered systems, *Phys. Rev. Lett.* **47**, 1546 (1981).
- [18] A. MacKinnon and B. Kramer, The scaling theory of electrons in disordered solids: Additional numerical results, *Z. Phys. B* **53**, 1 (1983).
- [19] K. Slevin and T. Ohtsuki, Corrections to scaling at the Anderson transition, *Phys. Rev. Lett.* **82**, 382 (1999).
- [20] A. Rodriguez, L. J. Vasquez, K. Slevin, and R. A. Römer, Critical parameters from a generalized multifractal analysis at the Anderson transition, *Phys. Rev. Lett.* **105**, 046403 (2010).
- [21] M. Lopez, J.-F. m. c. Clément, P. Szriftgiser, J. C. Garreau, and D. Delande, Experimental test of universality of the Anderson transition, *Phys. Rev. Lett.* **108**, 095701 (2012).
- [22] K. Slevin and T. Ohtsuki, Critical exponent for the Anderson transition in the three-dimensional orthogonal universality class, *New Journal of Physics* **16**, 015012 (2014).
- [23] E. Tarquini, G. Biroli, and M. Tarzia, Critical properties of the Anderson localization transition and the high-dimensional limit, *Phys. Rev. B* **95**, 094204 (2017).
- [24] T. Devakul and D. A. Huse, Anderson localization transitions with and without random potentials, *Phys. Rev. B* **96**, 214201 (2017).
- [25] K. Slevin and T. Ohtsuki, Critical exponent of the Anderson transition using massively parallel supercomputing, *J. Phys. Soc. Jpn.* **87**, 094703 (2018).
- [26] X. Luo and T. Ohtsuki, Universality classes of the Anderson transitions driven by quasiperiodic potential in the three-dimensional Wigner-Dyson symmetry classes, *Phys. Rev. B* **106**, 104205 (2022).
- [27] P. Sierant, D. Delande, and J. Zakrzewski, Thouless time analysis of Anderson and many-body localization transitions, *Phys. Rev. Lett.* **124**, 186601 (2020).
- [28] J. Šuntajs, T. Prosen, and L. Vidmar, Spectral properties of three-dimensional Anderson model, *Ann. Phys.* **435**, 168469 (2021).
- [29] J. Šuntajs, T. Prosen, and L. Vidmar, Localization challenges quantum chaos in the finite two-dimensional Anderson model, *Phys. Rev. B* **107**, 064205 (2023).
- [30] C. Vanoni, B. L. Altshuler, V. E. Kravtsov, and A. Scardicchio, Renormalization group analysis of the Anderson model on random regular graphs, *Proceedings of the National Academy of Sciences* **121** (2024).
- [31] B. L. Altshuler, V. E. Kravtsov, A. Scardicchio, P. Sierant, and C. Vanoni, Renormalization group for Anderson localization on high-dimensional lattices, [arXiv:2403.01974](https://arxiv.org/abs/2403.01974).
- [32] I. García-Mata, O. Giraud, B. Georgeot, J. Martin, R. Dubertrand, and G. Lemarié, Scaling theory of the Anderson transition in random graphs: Ergodicity and universality, *Phys. Rev. Lett.* **118**, 166801 (2017).
- [33] I. García-Mata, J. Martin, R. Dubertrand, O. Giraud, B. Georgeot, and G. Lemarié, Two critical localization lengths in the Anderson transition on random graphs, *Phys. Rev. Res.* **2**, 012020 (2020).
- [34] M. Pino, Scaling up the Anderson transition in random-regular graphs, *Phys. Rev. Res.* **2**, 042031 (2020).
- [35] I. García-Mata, J. Martin, O. Giraud, B. Georgeot, R. Dubertrand, and G. Lemarié, Critical properties of the Anderson transition on random graphs: Two-parameter scaling theory, Kosterlitz-Thouless type flow, and many-body localization, *Phys. Rev. B* **106**, 214202 (2022).
- [36] P. Sierant, M. Lewenstein, and A. Scardicchio, Universality in Anderson localization on random graphs with varying connectivity, *SciPost Phys.* **15**, 045 (2023).
- [37] J. M. Kosterlitz, Kosterlitz-Thouless physics: a review of key issues, *Reports on Progress in Physics* **79**, 026001 (2016).
- [38] B. L. Altshuler, Y. Gefen, A. Kamenev, and L. S. Levitov, Quasiparticle lifetime in a finite system: A nonperturbative approach, *Phys. Rev. Lett.* **78**, 2803 (1997).
- [39] D. Basko, I. Aleiner, and B. Altshuler, Metal-insulator transition in a weakly interacting many-electron system with localized single-particle states, *Ann. Phys. (N.Y.)* **321**, 1126 (2006).
- [40] S. Roy and D. E. Logan, The Fock-space landscape of many-body localisation, *Journal of Physics: Condensed Matter* **37**, 073003 (2024).
- [41] J. Šuntajs, J. Bonča, T. Prosen, and L. Vidmar, Quantum chaos challenges many-body localization, *Phys. Rev. E* **102**, 062144 (2020).
- [42] J. Šuntajs, J. Bonča, T. Prosen, and L. Vidmar, Ergodicity breaking transition in finite disordered spin chains, *Phys. Rev. B* **102**, 064207 (2020).
- [43] T. LeBlond, D. Sels, A. Polkovnikov, and M. Rigol, Universality in the onset of quantum chaos in many-body systems, *Phys. Rev. B* **104**, L201117 (2021).
- [44] H. Kim and A. Polkovnikov, Integrability as an attractor of adiabatic flows, *Phys. Rev. B* **109**, 195162 (2024).
- [45] B. Bhattacharjee, A. Andrianov, and S. Flach, Thermalization slowing down of weakly nonintegrable quantum spin dynamics, [arXiv:2405.00786](https://arxiv.org/abs/2405.00786).
- [46] R. K. Panda, A. Scardicchio, M. Schulz, S. R. Taylor, and M. Žnidarič, Can we study the many-body localisation transition?, *EPL* **128**, 67003 (2019).
- [47] P. Sierant, M. Lewenstein, and J. Zakrzewski, Polynomially filtered exact diagonalization approach to many-body localization, *Phys. Rev. Lett.* **125**, 156601 (2020).
- [48] N. Laflorencie, G. Lemarié, and N. Macé, Chain breaking and Kosterlitz-Thouless scaling at the many-body localization transition in the random-field Heisenberg spin chain, *Phys. Rev. Research* **2**, 042033 (2020).
- [49] D. Sels and A. Polkovnikov, Dynamical obstruction to localization in a disordered spin chain, *Phys. Rev. E* **104**, 054105 (2021).
- [50] D. Sels and A. Polkovnikov, Thermalization of dilute impurities in one-dimensional spin chains, *Phys. Rev. X* **13**, 011041 (2023).
- [51] J. Niedda, G. B. Testasecca, G. Magnifico, F. Balducci, C. Vanoni, and A. Scardicchio, Renormalization-group analysis of the many-body localization transition in the random-field xxz chain, [arXiv:2410.12430](https://arxiv.org/abs/2410.12430).
- [52] V. Oganesyan and D. A. Huse, Localization of interacting fermions at high temperature, *Phys. Rev. B* **75**, 155111 (2007).
- [53] M. Žnidarič, T. Prosen, and P. Prelovšek, Many-body localization in the Heisenberg XXZ magnet in a random field, *Phys. Rev. B* **77**, 064426 (2008).
- [54] A. De Luca and A. Scardicchio, Ergodicity breaking in a model showing many-body localization, *Europhysics Letters* **101**, 37003 (2013).
- [55] F. Alet and N. Laflorencie, Many-body localization: An introduction and selected topics, *C. R. Phys.* **19**, 498

- (2018).
- [56] D. A. Abanin, E. Altman, I. Bloch, and M. Serbyn, Colloquium: Many-body localization, thermalization, and entanglement, *Rev. Mod. Phys.* **91**, 021001 (2019).
- [57] M. Kliczkowski, R. Świątek, M. Hopjan, and L. Vidmar, Fading ergodicity, *Phys. Rev. B* **110**, 134206 (2024).
- [58] L. D’Alessio, Y. Kafri, A. Polkovnikov, and M. Rigol, From quantum chaos and eigenstate thermalization to statistical mechanics and thermodynamics, *Adv. Phys.* **65**, 239 (2016).
- [59] J. Šuntajs and L. Vidmar, Ergodicity Breaking Transition in Zero Dimensions, *Phys. Rev. Lett.* **129**, 060602 (2022).
- [60] J. Šuntajs, M. Hopjan, W. De Roeck, and L. Vidmar, Similarity between a many-body quantum avalanche model and the ultrametric random matrix model, *Phys. Rev. Res.* **6**, 023030 (2024).
- [61] W. De Roeck and F. Huveneers, Stability and instability towards delocalization in many-body localization systems, *Phys. Rev. B* **95**, 155129 (2017).
- [62] D. J. Luitz, F. Huveneers, and W. De Roeck, How a small quantum bath can thermalize long localized chains, *Phys. Rev. Lett.* **119**, 150602 (2017).
- [63] T. Thiery, F. Huveneers, M. Müller, and W. De Roeck, Many-body delocalization as a quantum avalanche, *Phys. Rev. Lett.* **121**, 140601 (2018).
- [64] I.-D. Potirniche, S. Banerjee, and E. Altman, Exploration of the stability of many-body localization in $d > 1$, *Phys. Rev. B* **99**, 205149 (2019).
- [65] P. J. D. Crowley and A. Chandran, Avalanche induced coexisting localized and thermal regions in disordered chains, *Phys. Rev. Research* **2**, 033262 (2020).
- [66] P. J. D. Crowley and A. Chandran, Mean-field theory of failed thermalizing avalanches, *Phys. Rev. B* **106**, 184208 (2022).
- [67] D. Sels, Bath-induced delocalization in interacting disordered spin chains, *Phys. Rev. B* **106**, L020202 (2022).
- [68] A. Morningstar, L. Colmenarez, V. Khemani, D. J. Luitz, and D. A. Huse, Avalanches and many-body resonances in many-body localized systems, *Phys. Rev. B* **105**, 174205 (2022).
- [69] J. Léonard, S. Kim, M. Rispoli, A. Lukin, R. Schittko, J. Kwan, E. Demler, D. Sels, and M. Greiner, Probing the onset of quantum avalanches in a many-body localized system, *Nature Physics* **19**, 481 (2023).
- [70] K. Pawlik, P. Sierant, L. Vidmar, and J. Zakrzewski, Many-body mobility edge in quantum sun models, *Phys. Rev. B* **109**, L180201 (2024).
- [71] T. Szoldra, P. Sierant, M. Lewenstein, and J. Zakrzewski, Catching thermal avalanches in the disordered xxz model, *Phys. Rev. B* **109**, 134202 (2024).
- [72] A. Kutlin and C. Vanoni, Investigating finite-size effects in random matrices by counting resonances, [arXiv:2402.10271](https://arxiv.org/abs/2402.10271).
- [73] E. Bianchi, L. Hackl, M. Kieburg, M. Rigol, and L. Vidmar, Volume-Law Entanglement Entropy of Typical Pure Quantum States, *PRX Quantum* **3**, 030201 (2022).
- [74] See Supplemental Material for further details on numerical implementation of the model, the relationship between the entanglement entropy and matrix elements fluctuations, finite-size scaling of the entanglement entropies, and the numerical implementation of the beta function.
- [75] www.hpc-rivr.si.
- [76] eurohpc-ju.europa.eu.
- [77] www.izum.si.
- [78] M. Hopjan and L. Vidmar, Scale-invariant survival probability at eigenstate transitions, *Phys. Rev. Lett.* **131**, 060404 (2023).
- [79] M. Hopjan and L. Vidmar, Scale-invariant critical dynamics at eigenstate transitions, *Phys. Rev. Res.* **5**, 043301 (2023).
- [80] A. T. James, Distributions of Matrix Variates and Latent Roots Derived from Normal Samples, *The Annals of Mathematical Statistics* **35**, 475 (1964).

End matter

Appendix A: Quantum sun model.— The quantum sun model consists of a thermal inclusion (a quantum dot) with $N = 3$ spins, and L localized spins outside the dot. The Hamiltonian for this model can be written as

$$\hat{H} = \hat{R} + g_0 \sum_{\ell=0}^{L-1} \alpha^{u_\ell} \hat{S}_{n(\ell)}^x \hat{S}_\ell^x + \sum_{\ell=0}^{L-1} h_\ell \hat{S}_\ell^z, \quad (14)$$

where the thermal dot is modeled by a normalized all-to-all random matrix \hat{R} drawn from the Gaussian orthogonal ensemble (GOE) [60, 74]. The spins outside the dot are subject to on-site disorder $h_\ell \in [0.5, 1.5]$ drawn from a uniform distribution. The interaction term connects a localized spin at site ℓ to a randomly selected spin in the dot, $n(\ell)$, via an exponentially decaying strength $g_0 \alpha^{u_\ell}$ with $u_\ell \in [\ell - 0.2, \ell + 0.2]$. Decreasing the interaction α drives the model from an ergodic phase at $\alpha > \alpha_c$, through an ergodicity breaking phase transition at $\alpha = \alpha_c$, to a Fock-space localized phase for $\alpha < \alpha_c$ [59, 60, 78, 79]. Following

previous theoretical arguments, the transition occurs at $\alpha_c = 1/\sqrt{2} \approx 0.707$ [61, 62], while the numerical results suggest the transition to occur at slightly larger α_c , which may also depend on g_0 [60]. We study this model for system sizes up to $L + N = 19$, see also [74] for further details about the numerical implementation.

Appendix B: Scaling collapse at the critical point.— In Fig. 4(a) we show additional results for the behavior of s vs α in the vicinity of the critical point for various system sizes L and parameters g_0 . As expected, $s_c \rightarrow 0$ as $g_0 \rightarrow 0$ and $s_c \rightarrow 1$ as $g_0 \rightarrow 1$. We then find the scaling collapses using the cost function minimization [42], see [74] for details. Here we consider the correlation length ξ consistent with fading ergodicity, *i.e.*, $\xi = \eta^\nu \sim \left[\ln(\alpha/\alpha_c) \right]^{-\nu}$, where ν is the critical exponent. While we expect $\nu = 1$ in the thermodynamic limit (as argued in the main text), the results in finite systems may give rise to $\nu \neq 1$.

The cost function minimization gives rise to the optimal values of the critical exponent ν , the critical point

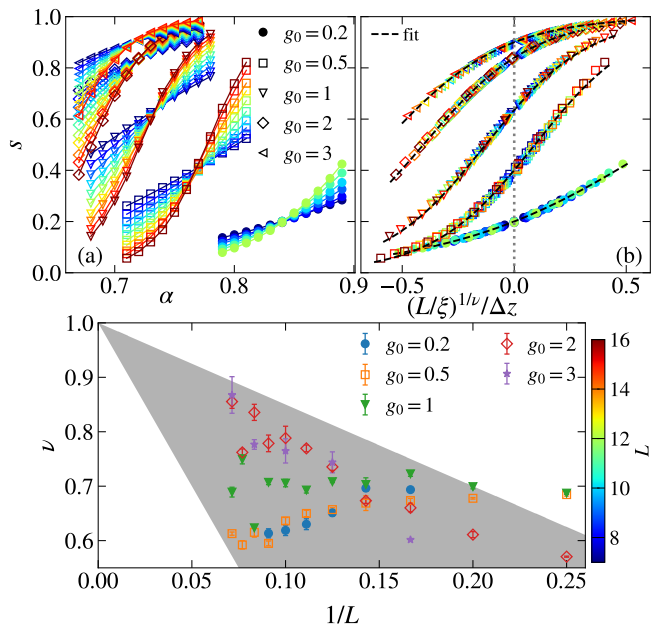


FIG. 4. (a) Entanglement entropy s vs α in the vicinity of the critical point, for different system sizes L and values of g_0 . (b) Scaling collapses using a cost function minimization for the values of α shown in panel (a). The dashed line denotes a fit of Eq. (7) to the collapsed results, *i.e.*, upon exchanging $L/\eta \rightarrow (L/\xi)^{1/\nu}$. We normalize the values on the x-axis by $\Delta z = \max(L/\xi)^{1/\nu} - \min(L/\xi)^{1/\nu}$ to show different g_0 on the same scale. (c) Critical exponent ν as a function of the inverse of system size $1/L$, obtained by the procedure described in the main text.

α_c , and the entropy at the critical point s_c . The resulting scaling collapses are shown in Fig. 4(b), while the values of ν , α_c and s_c , as well as the quality of the scaling collapses, are listed in Sec. S3 of [74]. In general, we find better scaling collapses at large g_0 , for which the critical point α_c is closer to the analytically predicted value $\alpha_c = 1/\sqrt{2}$, and the critical exponent ν is closer to $\nu = 1$. In the numerical analysis, the critical exponent is smaller than the theoretically predicted $\nu = 1$. Using Eq. (13), we estimate $\nu = 1 - L_0/L \in (0.6, 0.8)$ (since $L_0 \in (3, 6)$ in Fig. 2), which is in good agreement with the values given from the scaling collapses.

We complement our analysis by estimating the corrections to the critical exponent ν , namely, we calculate the critical exponent as a function of system size. For a given L , we perform a finite-size collapse using system sizes in the range $[L - 1, L + 2]$ and vary L across the available data points. We use the same correlation length $\xi = \eta^\nu$ as in Fig. 4(b). The resulting critical exponents are shown in Fig. 4(c) as a function of $1/L$. For large values of $g_0 > 1$ we find remarkable agreement with our framework described in the main text. We estimate $L_0 \sim 3$ from the results. However, the smaller values of $g_0 < 1$ show large finite size effects and it is not clear whether the flow of the critical exponent ν will resume

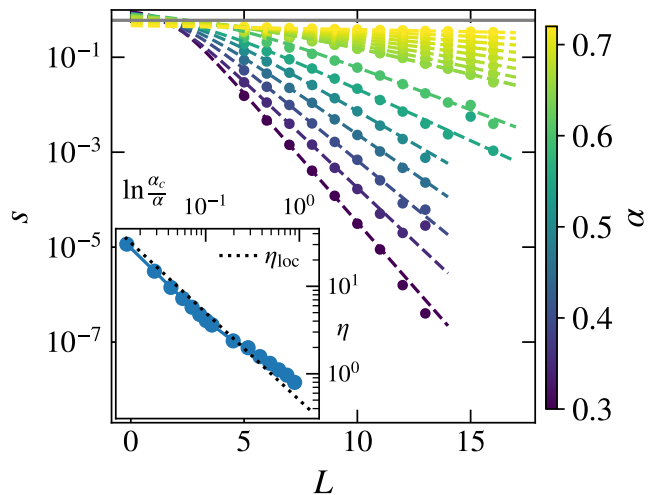


FIG. 5. Entanglement entropy s vs L at $g_0 = 1$, in the localized regime $\alpha < \alpha_c$. The dashed curves are fits from Eq. (7) to sizes $L \geq 7$. Inset: Correlation length η obtained from the fits in the main panel. The dotted line shows the prediction from Ref. [59].

$1 - L_0/L$ corrections at large L or whether ν remains smaller, giving rise to $\nu < 1$ in the thermodynamic limit.

Appendix C: Scaling in the localized regime. — We complement our results by studying the properties of the beta function in the localized phase. We show in Fig. 5 that the numerical results for s are in good agreement with the ansatz from Eq. (7). In the inset of Fig. 5, we plot the resulting localization length η_{loc} , showing that it agrees with the prediction $\eta_{\text{loc}} = 1/\ln(\alpha_c/\alpha)^2$. The observed scaling behavior of s is consistent with the beta function in Eq. (6) in the limit $s \rightarrow 0$, as argued in the main text.

Supplemental Material: Scaling theory of fading ergodicity

Rafał Świątek^{1,2}, Miroslav Hopjan¹, Carlo Vanoni^{3,4}, Antonello Scardicchio^{5,6} and Lev Vidmar^{1,2}

¹*Department of Theoretical Physics, J. Stefan Institute, SI-1000 Ljubljana, Slovenia*

²*Department of Physics, Faculty of Mathematics and Physics, University of Ljubljana, SI-1000 Ljubljana, Slovenia*

³*SISSA – International School for Advanced Studies, via Bonomea 265, 34136, Trieste, Italy*

⁴*Department of Physics, Princeton University, Princeton, New Jersey, 08544, USA*

⁵*INFN Sezione di Trieste, Via Valerio 2, 34127 Trieste, Italy*

⁶*ICTP, Strada Costiera 11, 34151, Trieste, Italy*

S1. NUMERICAL IMPLEMENTATION OF THE MODEL

Here we comment on the numerical implementation of the quantum sun model Hamiltonian defined in Eq. (14) of End Matter. We model the thermal quantum dot with a normalized $2^N \times 2^N$ matrix from a Gaussian orthogonal ensemble (GOE), defined as

$$R = \frac{R_0}{\sqrt{2^N + 1}}, \quad (\text{S1})$$

where $R_0 = (A + A^T)/2$, with A being a random matrix with elements distributed from a normal distribution. The matrix R from Eq. (S1) has a unit Hilbert-Schmidt norm [60]. Then, the corresponding operator of the Hamiltonian is a tensor product of R with an identity operator acting on L spins outside the dot, *i.e.*, $\hat{R} = R \otimes \mathcal{I}$. The spins outside the dot are coupled to a randomly selected spin within the dot. We set the coupling of the first spin outside the dot to $\alpha^{u_0} = 1$, *i.e.*, $u_0 = 0$, while the remaining $u_{\ell \geq 1}$ are drawn uniformly from the interval $[\ell - 0.2, \ell + 0.2]$.

Numerical results for the entanglement entropy s are obtained by carrying out an average over \mathcal{N}_{av} Hamiltonian realizations. We use $\mathcal{N}_{av} \geq 5000$ realizations for $L + N \leq 12$, $\mathcal{N}_{av} = 4000$ realizations for $L + N = 13, 14$, $\mathcal{N}_{av} \geq 1500$ disorder realizations for $L + N = 15$, and $\mathcal{N}_{av} \geq 500$ for $L + N = 16$. For system sizes beyond full exact diagonalization (ED) we employ polynomially filtered ED (POLFED) [47] to target $N_{eig} = 500$ central eigenvalues with a tolerance of $\delta = 10^{-14}$. In this case we use $\mathcal{N}_{av} \geq 500$ realizations for $L + N = 17$ and 18, while for $L + N = 19$ we perform $\mathcal{N}_{av} \geq 200$ averages.

S2. ENTANGLEMENT ENTROPY VS MATRIX ELEMENTS

Let us write a general state $|\psi\rangle$ of a system of L spins-1/2 in the basis of product states that are eigenstates of

the local magnetization operator \hat{S}_ℓ^z ,

$$|\psi\rangle = \sum_{k=1}^D c_k |k\rangle, \quad (\text{S2})$$

where $|k\rangle \in (\mathbb{C}^2)^{\otimes L}$ are the basis states and $c_k = \langle k|\psi\rangle$ is the coefficient of the wavefunction. In this work, we are interested in the properties of a single spin. The basis $\{|k\rangle\}$ can be decomposed in the basis $|b\rangle \otimes |\sigma\rangle$, where $|b\rangle \in (\mathbb{C}^2)^{\otimes L-1}$ and $|\sigma\rangle \in \mathbb{C}^2 = \{|\downarrow\rangle, |\uparrow\rangle\}$. Hence, our state takes the form

$$|\psi\rangle = \sum_b \sum_\sigma c_{b\sigma} |b\rangle \otimes |\sigma\rangle. \quad (\text{S3})$$

Next, we can find the reduced density matrix for the single spin on site ℓ and trace out the remaining degrees of freedom, *i.e.*,

$$\begin{aligned} \hat{\rho}_\ell &= \text{Tr}_B |\psi\rangle\langle\psi| \\ &= \sum_{b''} \sum_{b, b'} \sum_{\sigma, \sigma'} c_{b\sigma} c_{b'\sigma'}^* \langle b'' | (|b\rangle \otimes |\sigma\rangle \langle\sigma'| \otimes \langle b'|) | b'' \rangle \\ &= \sum_{\sigma, \sigma'} \sum_b c_{b\sigma} c_{b\sigma'}^* |\sigma\rangle\langle\sigma'| = \begin{pmatrix} A_{00} & A_{01} \\ A_{10} & A_{11} \end{pmatrix}, \end{aligned} \quad (\text{S4})$$

where $A_{\sigma\sigma'} = \sum_b c_{b\sigma} c_{b\sigma'}^*$. Due to the property $\text{Tr}\{\hat{\rho}_\ell\} = 1$, we have $A_{11} = 1 - A_{00}$ and we set $A_{01} = A_{10}^*$ due to hermiticity of the density matrix. The eigenvalues of the matrix $\hat{\rho}_\ell$ can be then expressed as

$$\lambda_\pm = \frac{1}{2} \pm \frac{1}{2} \sqrt{(1 - 2A_{00})^2 + 4|A_{01}|^2}. \quad (\text{S5})$$

On the other hand, the expectation value z of the local magnetization \hat{S}_ℓ^z can be found in a similar manner,

$$\begin{aligned} z \equiv \langle\psi|\hat{S}_\ell^z|\psi\rangle &= \sum_{b, b'} \sum_{\sigma, \sigma'} c_{b'\sigma'}^* c_{b\sigma} \langle b'| \otimes \langle\sigma'| \hat{S}_\ell^z |\sigma\rangle \otimes |b\rangle \\ &= \sum_{\sigma, \sigma'} \sum_b c_{b\sigma}^* c_{b\sigma} \underbrace{\langle\sigma'|\hat{S}_\ell^z|\sigma\rangle}_{\sigma \cdot \delta\sigma'} \\ &= \frac{1}{2} A_{11} - \frac{1}{2} A_{00} = \frac{1}{2} - A_{00}, \end{aligned} \quad (\text{S6})$$

where we choose the spin- $\frac{1}{2}$ eigenvalues $\sigma \in \{-\frac{1}{2}, \frac{1}{2}\}$. Following a similar calculation one can additionally find that the off-diagonal elements of the reduced density matrix become

$$A_{01} = \langle \psi | \hat{S}_\ell^- | \psi \rangle = \langle \psi | \hat{S}_\ell^x - i \hat{S}_\ell^y | \psi \rangle \equiv x - iy. \quad (\text{S7})$$

Remarkably, this indicates that the eigenvalues λ_\pm of the reduced density matrix are related to the fluctuations of matrix elements at the same site,

$$\lambda_\pm = \frac{1}{2} \left(1 \pm 2\sqrt{|x|^2 + |y|^2 + |z|^2} \right). \quad (\text{S8})$$

For a $U(1)$ symmetric system, the off-diagonals of the reduced density matrix disappear, *i.e.*, $x = y = 0$. We can then write the single-site entanglement entropy S for the state $|\psi\rangle$ as

$$\begin{aligned} S &= -\text{Tr}(\hat{\rho}_\ell \ln \hat{\rho}_\ell) \\ &= -\left(\frac{1}{2} - \frac{z}{4}\right) \ln\left(\frac{1}{2} - \frac{z}{4}\right) - \left(\frac{1}{2} + \frac{z}{4}\right) \ln\left(\frac{1}{2} + \frac{z}{4}\right). \end{aligned} \quad (\text{S9})$$

In the ETH regime at infinite temperature, one can assume a vanishingly small value of the magnetization, such that we can expand the above expression at $z = 0$ to get

$$S \approx \ln 2 - 2z^2 + O(z^4). \quad (\text{S10})$$

Consequently, we find that the average of entanglement entropies over some states ψ (e.g., the Hamiltonian eigenstates) are directly related to the variance of diagonal matrix elements over the same set of states.

Similar considerations apply for models without $U(1)$ symmetry, where the off-diagonal terms of the reduced density matrix A_{01} modify Eq. (S10) to

$$\begin{aligned} S &\approx |u| \ln \frac{1 - 2|u|}{1 + 2|u|} - \frac{1}{2} \ln \left(\frac{1}{4} - |u|^2 \right) \\ &\quad + \frac{1}{2|u|} \ln \left(\frac{1 - 2|u|}{1 + 2|u|} \right) z^2 + O(z^4), \end{aligned} \quad (\text{S11})$$

with $u = A_{01}$. As argued in [57], fading ergodicity manifests itself for certain physical observables, such as \hat{S}_ℓ^z , as softening of fluctuations of matrix elements, *i.e.*, the matrix elements fluctuations are larger than those predicted by the ETH. On the other hand, other observables such as those that include the operator \hat{S}_ℓ^x still exhibit faster (ETH-like) decay of fluctuations. Hence, we expect fluctuations of S in Eq. (S11) to be governed by z . Sending $u \rightarrow 0$ in Eq. (S11) while keeping $z > 0$ gives rise to the same expression as given in Eq. (S10).

S3. FINITE-SIZE SCALING OF THE ENTANGLEMENT ENTROPY

A. Results for random pure states

Within the random matrix theory, the distribution for the eigenvalues of the reduced density matrix is the

Wishart distribution, which for a generic parameter β (not to be confused with the beta function) takes the form [80]

$$\begin{aligned} d\mu &= \frac{1}{Z^\beta} d^N \lambda \prod_{i < j} |\lambda_i - \lambda_j|^\beta \\ &\quad \times \prod_l \lambda_l^{[(1+M-N)-2/\beta]\beta/2} \delta(1 - \sum_k \lambda_k), \end{aligned} \quad (\text{S12})$$

where the $SO(N)$ volume has been dropped and $\lambda_i > 0$, $\forall i$. In our case, we have to consider a GOE matrix ($\beta = 1$) of dimension \mathcal{D} , where the reduced density matrices of the subsystems have dimension $N = 2$ and $M = \mathcal{D}/N$. This gives

$$d\mu = \frac{1}{Z} d\lambda_1 d\lambda_2 |\lambda_1 - \lambda_2| \lambda_1^{\frac{\mathcal{D}-6}{4}} \lambda_2^{\frac{\mathcal{D}-6}{4}} \delta(1 - \lambda_1 - \lambda_2), \quad (\text{S13})$$

with

$$Z = \frac{2^{6-\mathcal{D}}}{\mathcal{D}-2}. \quad (\text{S14})$$

The entanglement entropy is then $s = -(\lambda_1 \ln \lambda_1 + \lambda_2 \ln \lambda_2) / \ln 2$, so the average can be computed as

$$\langle s \rangle = -\frac{2}{\ln 2} \int d\mu \lambda_1 \ln(\lambda_1). \quad (\text{S15})$$

Since the measure $d\mu$ in Eq. (S13) contains an absolute value, it is convenient to split the integral into two parts, $\langle s \rangle = 2(I_1 + I_2) / \ln 2$, of the form

$$I_1 = -\frac{1}{Z} \int_0^{1/2} d\lambda (1 - 2\lambda) (\lambda - \lambda^2)^n \lambda \ln \lambda \quad (\text{S16})$$

and

$$I_2 = -\frac{1}{Z} \int_{1/2}^1 d\lambda (2\lambda - 1) (\lambda - \lambda^2)^n \lambda \ln \lambda, \quad (\text{S17})$$

where we also set $n = (\mathcal{D}-6)/4$. To solve the integrals we introduce a change of variables, such that we can recast I_1 as

$$I_1 = -\frac{n+1}{2} \int_0^1 dy y^n \lambda_-(y) \ln \lambda_-(y), \quad (\text{S18})$$

and I_2 as

$$I_2 = -\frac{n+1}{2} \int_0^1 dy y^n \lambda_+(y) \ln \lambda_+(y), \quad (\text{S19})$$

where $\lambda_\pm = (1 \pm \sqrt{1-y})/2$. In the large n limit (corresponding to the large \mathcal{D} limit), both integrals are dominated by the contribution near $y = 1$, so we can expand in the small parameter $\epsilon = 1 - y$. In the expansion, the odd powers in I_1 and I_2 cancel, while the even powers sum and one gets, for $\mathcal{D} \gg 1$,

$$\langle s \rangle = 1 - \frac{2}{\mathcal{D}} + O\left(\frac{1}{\mathcal{D}^2}\right). \quad (\text{S20})$$

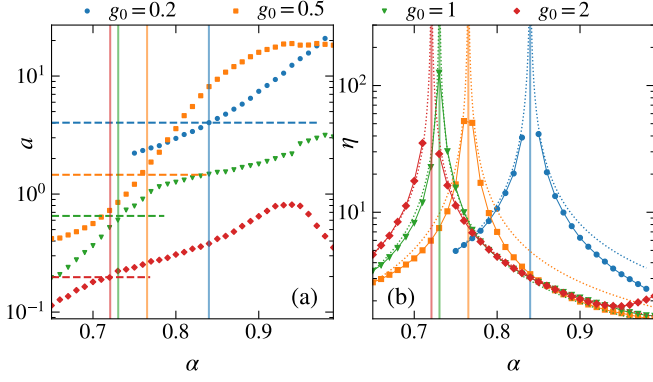


FIG. S1. (a) and (b) Fitting constants a and η from Eq. (S21), respectively, for different values of g_0 as a function of α . The vertical solid lines show the critical interaction α_c , while the horizontal dashed lines in (a) show $a_0 = 1/s_c - 1$ for different values of g_0 (marked by the same color), extracted from the data collapse in the main text (see End Matter). The dotted lines in (b) show the fit of $\bar{\eta}(\alpha) = b|\ln(\alpha/\alpha_c)|^{-1}$ to the numerical results for η vs α , where b is a fitting parameter.

When considering a physical Hamiltonian instead of the GOE matrix, $\mathcal{D} \rightarrow D$ is the Hilbert-space dimension. Then, the leading term of the random matrix theory prediction for the fluctuations of the entanglement entropy is proportional to $1/D$, as argued in the main text.

B. Numerical tests for the scaling ansatz

Here we test the ansatz for the finite-size scaling of the entanglement entropy in the quantum sun model,

$$s(L) = \frac{1}{1 + ae^{-L/\eta}}, \quad (\text{S21})$$

which is Eq. (7) in the main text. We show the results, at different values of g_0 , for a vs α in Fig. S1(a) and η vs α in Fig. S1(b).

In Fig. S1(a) we find $a \rightarrow a_0 = 1/s_c - 1$ in the vicinity of the critical point, while $a > a_0$ in the ergodic regime. In Fig. S1(b) we find a clear tendency of the divergence of η in the vicinity of the critical point. We fit the numerical results for η with an ansatz obtained from the analysis of the matrix elements fluctuations of the operator \hat{S}_L^z in the fading ergodicity regime, see Fig. 3(d) of [57]. The agreement between the numerical results and the fitted function is remarkable, suggesting the similarity between the scaling properties of the variances of the matrix elements of \hat{S}_L^z and the eigenstate entanglement entropy s , as anticipated from the analysis in Sec. S2.

C. Scaling collapses in the critical regime

In Fig. 4(a) of the main text (see End Matter) we show results for s vs α in the vicinity of the critical point,

g_0	C_X	α_c	s_c	ν
0.5	0.354	0.768	0.408	0.597
1	0.146	0.734	0.605	0.691
2	0.065	0.721	0.836	0.790
3	0.033	0.716	0.909	0.807

TABLE S1. Summary of cost function analysis, see Eq. (S22), for s vs α and different L . The scaling collapses are shown in Fig. 4(b) of the main text. For a fixed g_0 , the fitting parameters are α_c , s_c and ν .

at various L and g_0 . The maximal system size under investigation depends on the value of g_0 : for $g_0 < 0.5$ we study up to $L + N = 15$ particles, for $g_0 = 3$ we study up to $L + N = 18$ particles, while for $g_0 = 0.5, 1, 2$ we study up to $L + N = 19$ particles.

In Fig. 4(b) we show the scaling collapses of the results in Fig. 4(a) obtained by using the cost function minimization from Ref. [42]. Here we briefly summarize the main steps of the cost function minimization. The cost function for the observable X is defined as

$$C_X = \frac{\sum_i |X_{i+1} - X_i|}{\max X - \min X} - 1, \quad (\text{S22})$$

such that the optimal collapse is given by $C_X = 0$. To carry out the cost function procedure, we employ the differential evolution algorithm from the Python `scipy.optimize` library. We utilize a population size of 10^2 with up to 10^3 iterations, and an absolute tolerance of 10^{-2} . Given the stochastic nature of this method, we perform over 100 realizations and use the typical values (i.e., geometric mean) of the fitting parameters.

The results of the cost function minimization are summarized in Table S1 for $g_0 = 0.5, 1, 2, 3$, which are the parameters for which we considered the largest system sizes. The best scaling collapses are found for large g_0 , for which the critical point α_c is closest to the analytically predicted value $\alpha_c = 1/\sqrt{2}$, and the critical exponent ν is closest to $\nu = 1$. These results reinforce our expectation in the discussion of Fig. 3 in the main text, namely, that the numerical results at large g_0 are closest to the asymptotic regime, while the results at small g_0 are subject to strong finite-size effects.

S4. NUMERICAL CALCULATION OF THE BETA FUNCTION

In our study in the main text, we consider finite systems of sizes up to $L + N = 19$. To ensure a smooth curve for the entanglement entropy, $s(L)$, we fit our results in

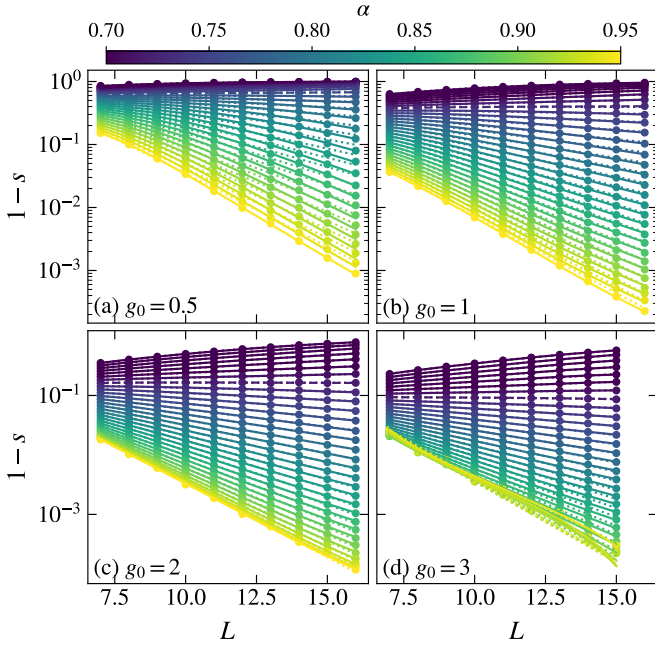


FIG. S2. Finite-size scaling of the subtracted entanglement entropy $1 - s$ vs L , for different values of g_0 . The solid lines represent the fits of Eqs. (S23) and (S24) using $x = \exp\{L/\eta\}$, while the dotted lines show the fit of Eq. (S21) to the results. The horizontal dashed line is the estimated critical point.

the ergodic regime (at $\alpha > \alpha_c$) to the Pade function F_1 ,

$$F_1(x) = \frac{x^2 + c_1x + c_0}{x^2 + d_1x + d_0}, \quad (\text{S23})$$

which ensures that $s \xrightarrow{L \rightarrow \infty} 1$, and in the localized regime (at $\alpha < \alpha_c$) to the Pade function F_2 ,

$$F_2(x) = \frac{c_3}{x^3} + \frac{c_2}{x^2} + \frac{c_1}{x} + \frac{d}{\sqrt{x}} + c_0, \quad (\text{S24})$$

such that $s \xrightarrow{L \rightarrow \infty} \text{const.}$ Since the corrections in the ergodic and localized regimes are exponential, the fitting variable should be $x \sim \exp\{L\}$. However, taking into account the fading ergodicity regime, a more relevant fitting parameter should be $x = \exp\{L/\eta\}$.

Following this method we are able to obtain smooth logarithmic derivatives of the interpolated results, which is central to the numerical calculation of the beta function. We fit the functions in Eqs. (S23) and (S24) to our results for s with $x = \exp\{L/\eta\}$, and we show the results in Fig. S2(a)-S2(d) for the whole range of α and different g_0 . Remarkably, the interpolated results fit the data points very well and reduce fluctuations due to the finite number of realizations. Alternatively, we fit Eq. (S21) to our results for all system sizes to test the validity of the ansatz. While in the asymptotic limit the fit seems to work remarkably well (see Fig. 2 of the main text), here we note that using Eq. (S23) we obtain a more robust fitting function for moderate system sizes. A natural explanation is that the expansion of Eq. (S23) contains corrections beyond Eq. (S21), which become relevant for smaller system sizes. Therefore, to evaluate the beta function it is more robust to choose the Pade function instead of the asymptotic scaling function expressed via Eq. (S21).